Adaptive Region Intensity Based Rigid Ultrasound and CT Image Registration

Zhijun Zhang
Surgery Department of the Chinese University of Hong Kong
Shatin, N.T., Hong Kong, China
alexzhang@surgery.cuhk.edu.hk

Abstract

Rigid registration of intraoperative ultrasound (US) and CT is an important technique to provide real-time guidance for preoperative images and models. Due to the speckle noise and artefacts in US images, accurate registration of CT and US is still a challenging problem. We propose an adaptive region intensity based CT and US registration method. The registration is initialized by matching the distinctive regions of CT and US images. Then the registration is a multistage process in which the regions in US used will be adaptively updated at each stage. The registration problem is considered as a global similarity energy optimization and high local statistical dependency regions selection process. Performances of our method and other intensity based method are evaluated with simulated and real datasets. Experiments results show the improvement of our registration method in robustness and accuracy.

1. Introduction

3D ultrasound (US) imaging is widely used in minimally invasive surgery due to its non-ionization, low cost and operating room friendly properties. It can help surgeon to localize the pathology during surgical planning and provide guidance for surgical tools during tumor resection and ablation. However, US images are spoiled by intrinsic speckle noise and artefacts such as shadows [2]. Sometimes it is difficult to delineate the anatomical or pathological information such as organ boundaries, vessels and tumors. To help surgeons comprehend the anatomical and pathological structures, a practical solution is to transform the preoperative CT information into the intraoperative US image space. Models extracted from preoperative CT images such as tumors and vessels can be augmented on the US images to provide surgical planning or guidance [1, 9]. This fusion of complementary information greatly improves surgical safety and performance. Multi-modal image registration is the essential technique to find the transform from CT to US image.

The multi-modal image registration can be categorized into model based, feature based and intensity based methods. Intensity based methods usually perform better since no feature or model extractions are needed and the registration accuracy is not limited by them. Maes *et al*. [12] proposed a mutual information (MI) based registration method. Studholme *et al*. [20] proposed an improvement of overlap independent method by using normalized mutual information (NMI). Roche *et al*. [17] proposed a method on correlation ratio (CR). In these methods, the transform is obtained by optimizing a similarity function which measures the statistical or functional dependency of two images.

The main drawback of intensity based multi-modal registration method is that when the registration starts with a large misalignment, there are a lot of local optima in the similarity function and the optimization method can easily be stuck to a local optimum. In papers on CT and US registration, the images usually need to be nearly aligned [15, 17], however, an initial transform is not always available. Moreover, for CT and US registration, these methods may not provide an accurate transform even when two images are close to alignment because the global optimum of the similarity function may not coincide with the correct alignment [3]. Finding regions with global distinctiveness and high statistical dependency will be the crucial problem for initialization and accurate registration. Globally distinctive regions can be detected by using feature extraction methods [8, 11] to assist the registration when there are noise or occlusions in the image. Feature based registration methods usually have larger capture range comparing with intensity based methods. Stewart *et al*. [19] proposed a method to register the retinal images by using local features. The registration starts from the matching between bootstrap regions and then propagates to global matching. However, these direct feature based methods are not suitable to find the initial matching between CT and US images because the local features in these images differ in location and scale. We need to develop an initial matching which tolerates some correspondence uncertainties. After a good initial matching, noisy and artefacts regions in US need to be excluded to avoid introduction of misleading optima into

978-1-4244-2243-2/08/$25.00 ©2008 IEEE

the similarity function. Many methods for removing the noisy areas have been proposed to improve the performance of similarity functions. Huang *et al*. [3] used a threshold to extract the cardiac wall regions in the US image. However, this simple operation does not work properly on US image with complex anatomical structures such as abdomen or brain. Leroy *et al*. [10] and Wein *et al*. [21] used shadow models to detect the artefacts regions. In real application, it is difficult to find a general model for artefacts to achieve good performances. Roche *et al*. [17] proposed a robust estimation of bivariate function together with a correlation ratio method to weight the noisy regions in US with smaller values. The results are usually dependent on the parameters tuning and the Powell's optimization process is time consuming. Penney *et al*. [16] extracted a vessel probability density map from the US images and used it to register with the MRI images. This method needs a learning process using a large amount of US images together with a manually determined threshold for MRI images. Ourselin *et al*. [14] proposed a robust registration method to estimate transform parameters from majority local matchings. They used equal block size for all local matchings, however, for some homogenous regions lack of structural information there will be matching ambiguities in local registrations. We develop a new method to select US regions with plentiful structure information and high statistical dependency to exclude the noisy and shadow areas.

The rest of the paper is organized as follows. Our propose adaptive region intensity based CT and US registration method is explained in Section 2. The experiments and datasets are introduced in Section 3. Results and discussion are shown in Section 4. Finally, conclusions are given in Section 5.

2. Method

2.1. Registration Framework

We propose a multistage registration method. In each stage a multi-resolution global matching is followed by many local matchings. The registration of CT to US is considered as a process of global similarity metric optimization and selection of high statistical dependency regions. The registration is initialized by a feature based matching of the distinctive regions. We choose US and CT images as fixed and moving images and the selected regions will be implemented as the mask of fixed image. The mask will be updated at each stage. We begin the first stage by using MI registration method with cone shape US mask and the initial parameters are obtained from feature region based matching. Local matchings initialized with the transform parameters from the global matching are then used to select the regions with high local statistical dependency. The selected regions will be joined and used as the mask for global registration of next stage. Polar coordinate sampling is used for MI calculation in global registration. Global and local registration will alternate until the global similarity is optimized. Fig.1 shows the collaboration of the global and local registration methods.

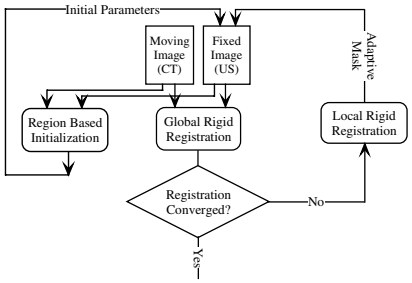

Figure 1. The combination of global and local rigid registrations.

2.2. Saliency Measurement

We use saliency to measure the distinctiveness of image regions [8]. Saliency is the measurement of both the local intensity unpredictability and the region dissimilarity over a scale. The scale can be considered as a sphere with a certain radius in 3D. The region saliency $S_D(x_0)$ around a voxel x_0 can be defined by the maximal local entropy H_D, weighted by a scale-space dissimilarity function W_D, which is the product of the optimal scale s_p and absolute difference of probability density function (PDF) over that scale:

$$S_D(s_p, x_0) = H_D(s_p, x_0) W_D(s_p, x_0), \tag{1}$$

with

$$W_D(s, x) = s \int_{i \in D} |\frac{\partial p_D(s, x)}{\partial s}| di, \tag{2}$$

and $p_D(s, x)$ is the PDF around x, i is the intensity variable which takes value in a set D.

Large saliency measurement means big unpredictability and salient change in scale-space, intuitively it means a region rich of structures and with low probability to be a dark shadow region. For homogenous or texture regions in the fixed image, it is usually difficult to register with the corresponding image because of lacking of corresponding information. Region saliency provides a way to find the optimum scale to include enough information for a local matching. We calculate the saliency value of each of the voxel. The optimum scale is searched between a scale range. Regions around the high saliency voxels can be used as features for initial matching. The feature regions should have a local support and each region center should be sufficient distant from the others.

2.3. Initialization

The locations and scales of saliency regions extracted from images with nonlinear intensity mapping such as US

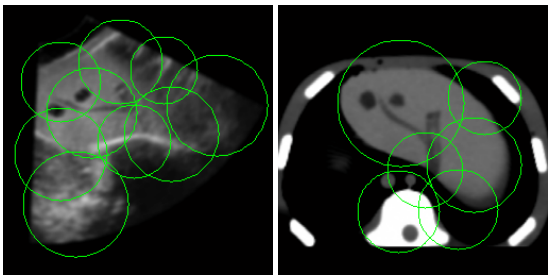

Figure 2. Saliency Regions extracted in US and CT Images.

and CT are usually different. Fig. 2 shows the saliency regions extracted from 2D CT and US images, the centers and radius of the circles show the location and scales of the saliency regions respectively.

We modify the feature based method [4] to find the initial transform between multi-modal images. Suppose we denote the US and CT images with I^f and I^m and N_f and N_m as feature regions extracted respectively. For each region $I_i^f (i = 1, ..., N_f)$ in the US, we try to register this sub-image with the CT image, initialized with a transform which brings the center of US sub-image to align with the center of each CT feature region $I_j^m (j = 1, ..., N_m)$. We optimize the MI metric between the sub-image of US with the CT image. After convergence, the image region in CT image with the largest similarity will be considered as the registered region of the US sub-image. Note most of the time, this CT region is different from any of the CT feature regions. Since the similarity metric is dependent on the image structure in both images, we can not compare the registered regions by their similarity values. We estimate the distinctiveness of the MI metric optimum of each registered region pair. Registered regions with high distinctiveness of optimum (DO) will be considered as regions with high statistical dependency. For each pair of the registered regions, (I_i^f, I_i^m), we denote the MI metric as $SM(I_i^f, T_i(I_i^m))$, with T_i the transform to map I_i^f with I_i^m. We then evaluate the MI metrics with K transforms whose magnitude of translational parameters errors from T_i are R, we denote the K similarity metrics as $SM(I_i^f, T_i^k(I_i^m))(k = 1, ...K)$. We verify if $SM(I_i^f, T_i(I_i^m))$ is larger than all of $SM(I_i^f, T_i^k(I_i^m))(k = 1, ...K)$, if this is not satisfied, this pair of registered regions will not be considered, otherwise, we will calculate DO by:

$$DO(i) = \frac{1}{K} \sum_{k=1}^{K} (SM(I_i^f, I_i^m) - SM(I_i^f, T_i^k(I_i^m)), i = 1, .., N \quad (3)$$

with N the number of registered regions to be considered. We choose all registered region pairs whose DO values are higher than the lower confidence limit of the group. In all of our experiments, we define the lower confidence limit of a sequence of value as $\mu - 2\sigma$, with μ and σ defined as the mean and the standard deviation of these values. These selected registered regions will be considered as the correspondence and an initial transform will be estimated by these corresponding regions.

2.4. Local Block Matching

In each stage, after a global registration with current mask is finished, high statistical dependency regions are selected by using local matchings. The whole US volume is divided into uniform blocks in polar coordinate and each block will be checked. The local blocks will be selected as components of the adaptively updated mask only if they pass the saliency, similarity and the similarity optimum distinctiveness tests sequentially.

We evaluate the saliency at each block center first. The saliency evaluated at the block center represents how much structure information inside it. The blocks with saliency values larger than the lower confidence limit will be used for local matching. We will then register the remain US blocks with the CT image initialized with the transform obtained from the global registration. The region around the block center with the optimal scale in saliency calculation as the radius is used for the local matching to include enough structure information. For each region, an MI based registration is used to acquire the local rigid transform and the sample points are extracted in Polar coordinate to calculate the joint PDF. When all of the local matchings are finished, we compare the NMI values of the registered regions, region pairs with NMI value larger than the lower confidence limit will be kept. Finally we check the DO values of the registered regions. The calculation of DO values is similar to that in the initialization step. Registered regions with DO values larger than the lower confidence limit will be considered as the high statistical dependency regions and the regions in US images will be joined as the mask. The local rigid transform parameters obtained from these selected blocks will be averaged and they will be passed to the global registration of next stage.

2.5. Implementation

In the initial matching, the optimal scale is searched between 50 and 120, 20 saliency regions are chosen for both the CT and US images. The DO values are calculated with 200 transforms whose translational parameters are uniformly located on a sphere of 10 with the translational parameters of registered regions as the center.

We use three stages for the adaptive region selection method. The initial block size is half of the image size in each dimensions and in each stages the block size is halved. We used Parzen window representation to evaluate the MI function as [13]. For MI and our methods, when evaluating the similarity metric, the number of histogram bins was 50. For the MI method and the first stage of our method, the

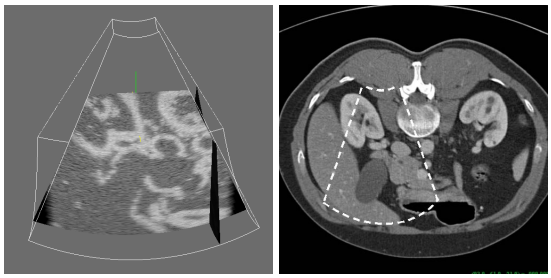

Figure 3. The simulated 3D US image and the original CT image.

number of samples points to calculate joint histogram was 50000, whereas in the following stages, the number of sample points was scaled by the ratio of the volume of current stage mask and the initial stage mask. In each of the block matching, the average number of sample points was 3000. We use steepest descent method to optimize the local and global similarity metrics.

3. Experiments and DataSets

The datasets in our experiments include simulated and real *in-vitro* and *in-vivo* 3D US images. The simulated US and CT image validation has the ground truth and the real data validation can provide results with real clinical consideration [6]. These validations are of complementary nature and can provide performance information of our method under different situations.

3.1. Simulated Dataset

We use Field II [7] ultrasound simulation package to generate the 3D US dataset. It can simulate transducers with any geometrical aperture and apodization scheme with linear excitation. We simulate a transducer with an array of 128 elements with center frequency of 7.5MHz, hanning apodization for both transmission and reception and with single focus point in transmission and multiple focus point in reception. The US dataset was simulated from a liver CT data with size of $512 \times 512 \times 370$ and voxel size of $0.65mm \times 0.65mm \times 0.65mm$. A region of interest (ROI) with size of $50mm \times 50mm \times 50mm$ is chosen for imaging. We generated a sequence of 2D sector plane US images to cover this 3D region. Each of the scan planes was tilted with an equal angle increase, and totally 63 planes are scanned with the total tilt angle $50°$. In each sector plane, 71 beams were used with total sector angle of $50°$. 3% of scatters were used to simulate the speckle pattern of biological tissue. The background scattering points were chosen randomly and the scattering points for bigger anatomical pattern come from the high gradient points in CT image. The simulated US dataset was then added with some shadow artefacts by setting noise intensities in Polar coordinate. The simulated US and the original CT datasets are shown in Fig. 3.

3.2. Real Data Acquisition

For real US data, we used both *in vitro* and *in vivo* datasets. The former came from a multi-modal abdominal phantom (model 057, CIRS Inc.), and the latter were from the abdominal images of five patients. All 3D US images were taken from a GE Voluson 730 machine with a 3D transducer of model RAB2-5L. The CT images were taken from a Helical CT machine of GE system. We use five pairs of phantom and patient images for our experiments. Two pairs of CT and US image characteristics for *in-vitro* and *in-vivo* experiments including image dimension, voxel size and number of datasets are shown in Table 1.

3.3. Experiments

The validation criteria include robustness and accuracy. They are evaluated by the capture range and the average transform parameters errors respectively. The capture range is the largest region inside which the registration can converge accurately starting from anywhere. The accuracy will be evaluated from the average errors of the parameters with the ground truth parameters. For simulated dataset, the ground truth was known. For each pair of the real images to be registered, a ground truth rigid transform was obtained by using a landmark initialized intensity based registration software. Several pairs of corresponding landmarks located in the whole image region were manually picked by a radiologist and then an MI based method with a manually labeled ROI refined the initial result. The registration was conducted until there was no noticeable misalignment between the transformed moving and fixed images by using visual inspection and then the ground truth parameters were obtained. We represent the 3D rigid transform by Euler transform. Each transform is represented by using six parameters, three for rotations and three for translations. For each criterion and for each dataset, we evaluated these parameters by running 300 registrations, each of which was initialized with an arbitrary transform. Each of the initial parameters was generated by adding an arbitrary displacement error of parameters to the ground truth parameters. In generating the arbitrary displacement error for parameters, each component of the parameters displacement was considered as a random variable with an uniform distribution. We chose the parameters so that initial average distance error [18] (ADE^i) was uniformly distributed between zero and a maximum value. In our experiments, ADE^i was defined with a cubic box of 100*mm* side length in the fixed image. In the capture range evaluation tests, the largest ADE^i was 50*mm*, the ranges for the translational and rotational errors were $\pm 40mm$ and $\pm 20°$, respectively. In the accuracy evaluation tests, the largest ADE^i was 40*mm* and the ranges for the translational and rotational error components were $\pm 30mm$ and $\pm 20°$ respectively.

Experiments	Data	Image Information	
		Dimension	Voxel size(mm)
in vitro	US phantom	$256 \times 256 \times 256$	$0.915 \times 0.708 \times 0.580$
	CT phantom	$256 \times 256 \times 119$	$1.25 \times 1.25 \times 1.25$
in vivo	US patient	$256 \times 256 \times 256$	$0.840 \times 0.591 \times 0.640$
	CT patient	$256 \times 256 \times 177$	$1.25 \times 1.25 \times 1.25$

Table 1. The *in vitro* and *in vivo* US and CT dataset characteristics.

The registration methods were implemented by using Insight Segmentation and Registration Toolkit 3.0 [5]. All the experiments were performed with a 3.2GHz Pentium IV PC with 1G MB memory. Typical executing time of MI based and our proposed registration method is 2 and 7 minutes.

4. Results and Discussion

4.1. Robustness

The capture ranges of both our proposed adaptive region MI (ARMI) and the MI based method are listed in Table 2. We can see the capture range of our method is larger than the MI based method, especially for the real subjects because shadows are more seriously in US images with complex structures. We search the initial correspondence using the saliency regions, the correspondences of these regions are globally distinctive, while the local minimum in similarity function varies with different regions considered in the MI based registration method, so our proposed method have a larger capture range than MI based method.

Experiments	Capture Range(mm)	
	MI	ARMI
simulated US to CT	33	40
phantom US to CT	38	46
patient US to CT	20	32

Table 2. The capture range of evaluated from different CT and US datasets. MI: mutual information registration method; ARMI: our proposed adaptive region MI based method.

4.2. Accuracy

We list the accuracy test results in Table 3. In both the simulated and real data experiments, the transform parameters errors with the ground truth are quite high after MI registration, while after our proposed method, the transform parameters errors with ground truth decreased greatly. For abdominal intraoperative surgery an allowable error should be within $5mm$, we can see our method can satisfy this requirement, while for MI based method it does not work.

4.3. Adaptive Regions Selection

We first show the simulated dataset result. The intensity in simulated US image has a good correlation with that in the CT image. After several shadows and noise are added to simulate the artefacts behind the bone, there will be new correspondence mode introduced into the joint PDF. This makes the MI reach optimum at different transform parameters than ground truth parameters. The first row of Fig. 4 shows the negative MI metrics evaluated at the alignment by using cone shape mask and the adaptive selected mask. (we use negative MI for all of our metric plots for illustration convenience.) The left images shows that when two images are aligned, the MI evaluated with whole US image mask is not maximized. The upper right image shows the improved metric plotting around the alignment parameters with the selected mask. Local block matching can help us to detect the artefacts regions, the left image of second row shows the adaptively selected US mask overlaid on the US image. We can see from this image all the shadow areas have been detected by the selected blocks. The final registration result is shown in the bottom right figure with US image overlaid on the gradient image of CT.

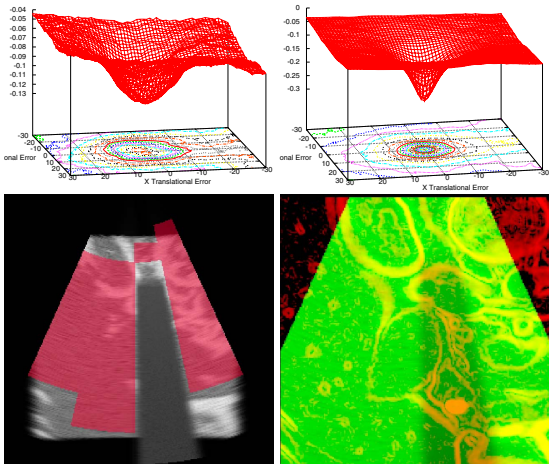

Figure 4. Results for registration of simulated ultrasound and CT dataset.

Registration of US and CT images of a phantom is shown in Fig. 5. The upper row shows the CT and US images. Images in the second row are the registration results by using MI based and our proposed method. The overlay of the transformed US images with CT images shows the improvement by our method. The similarity metrics against the x and y parameter errors are shown in the third row. The left figure corresponds to the similarity function (negative MI)

Experiments	Methods	Parameters Errors							
		Rotation(*rad*)				Translation(*mm*)			
		ΔR_x	ΔR_y	ΔR_z	$\|\|\Delta R\|\|$	ΔT_x	ΔT_y	ΔT_z	$\|\|\Delta T\|\|$
simulated US to CT	MI	0.025	0.039	0.053	0.07	0.49	3.16	4.57	5.57
	ARMI	0.021	0.026	0.038	0.05	0.28	0.55	0.96	1.13
US to CT phantom	MI	0.04	0.05	0.03	0.07	1.71	5.96	1.83	6.46
	ARMI	0.03	0.028	0.027	0.06	0.76	0.93	0.85	1.47
US to CT patients	MI	0.05	0.04	0.06	0.08	1.9	5.28	1.49	5.78
	ARMI	0.03	0.03	0.04	0.05	0.59	0.83	1.26	1.61

Table 3. The results of MI and our proposed registration method for the random initial parameters tests. MI: mutual information registration method; ARMI: our proposed adaptive region MI registration method.

using a cone shape mask, we can see the similarity function with cone mask evaluated at ground truth parameters is not the minimum value. The global registration by using whole US mask can only converge to a close position to alignment. We see in the right figure the similarity function evaluated with the adaptive mask after second stage. The similarity function is quite smooth and the minimum coincides with the alignment quite well. In the bottom row, the selected mask result after the second stage and the random sampled points for evaluating the MI in global registration are shown. We can see in the center right part of the US image, there is a shadow area inside which the correspondence of US with CT image is low, most of the blocks inside this region are removed by saliency, NMI value and optimum distinctiveness check.

Registration of a real subject abdominal images is shown in Fig.6. The top row shows the CT and US images of the patient liver. In the second row, from left to right are the registration results by using MI and our method displayed with color overlay. We can see the improvement of alignment near the inferior vena cava (IVC). The third row shows the similarity metrics plotted as functions of translational parameter errors in MI and our methods, we can see the optimum of MI with cone mask does not coincide with the alignment and the cost function is not very smooth, while with the adaptive selected mask, the optimum coincides with alignment well and the similarity function is quite smooth. The last row shows the selected regions in our method and the sample points used in the global MI calculation. We can see that the shadow region in the right part of the image is excluded from the registration.

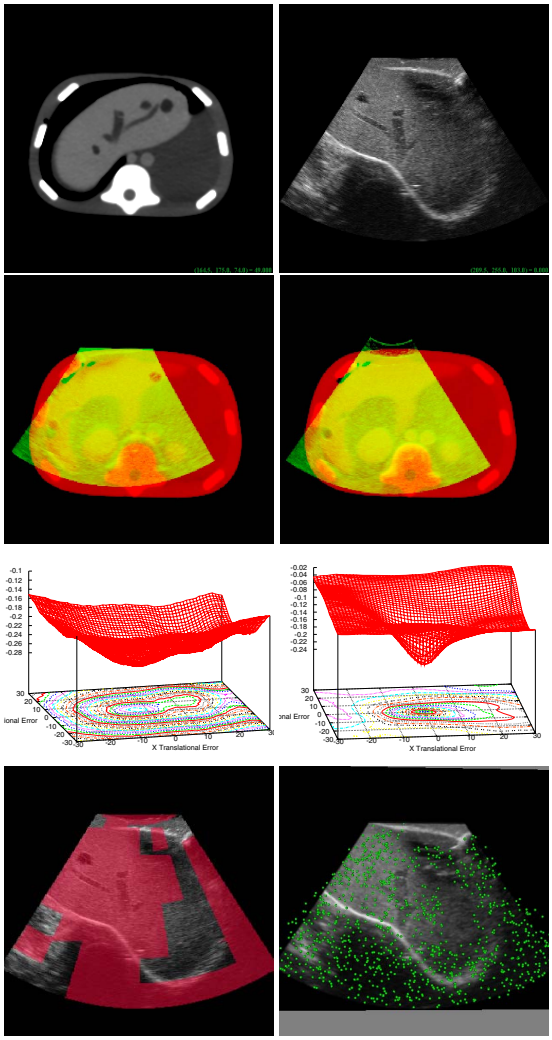

Figure 5. Phantom US to CT registration results by using MI and our methods. (Note in right image all the sample points before the plane are shown, so some points looks like have been selected from dark artefacts regions.)

5. Conclusion

In this paper, we have presented a new rigid CT to US image registration method. The regions with high saliency and similarity with CT image as useful information for registration have been adaptively selected. We have compared our method with typical intensity based multi-modal registration method. Registration results of simulated and real datasets show the improvement in terms of robustness and accuracy. The registration framework can be extended to non-rigid registration of CT and US images by replacing the

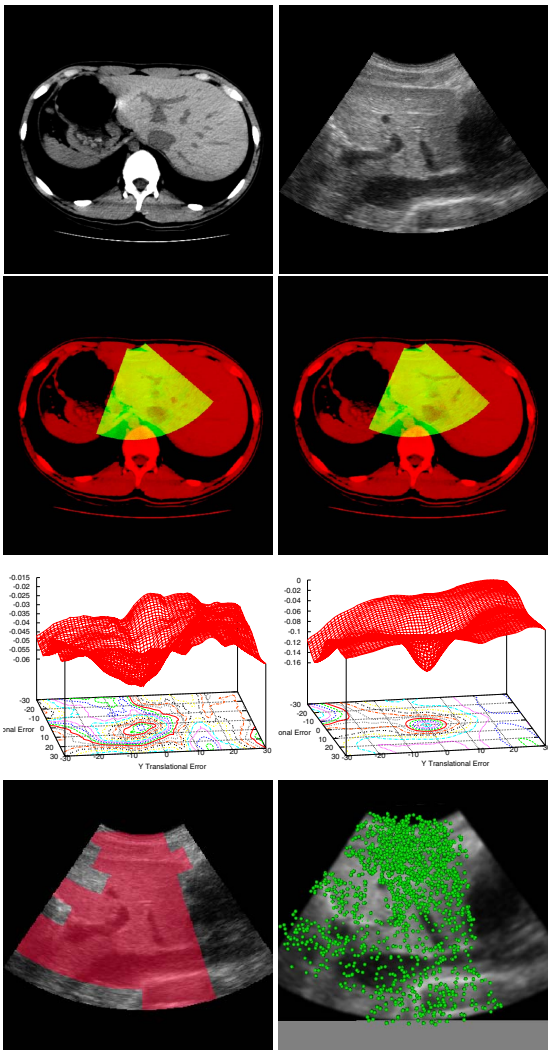

Figure 6. Registration results of US to CT patient liver by using MI and our proposed methods.

rigid transform with a B-spline based transform in global matching.

References

[1] S. Aylward, J. Jomier, J. Guyon, and S. Weeks. Intra-operative 3D ultrasound augmentation. In *Proc. IEEE ISBI*, pages 421–424, 2002. 1

[2] B. Block. *The Practice of Ultrasound – A Step by Step Guide to Abdominal Scanning*. Thieme Medical, 2004. 1

[3] X. Huang, N. Hill, J. Ren, and T. Peters. Dynamic 3D Ultrasound and MR image registration of the beating heart. In *Proc. MICCAI'05*, volume 3750, pages 171–178, 2005. 1, 2

[4] X. Huang, Y. Sun, D. Metaxas, F. Sauer, and C. Xu. Hybrid image registration based on configural matching of scale-invariant salient region features. In *Proc IEEE Workshop on Image and Video Registration*, pages 167–176, 2004. 3

[5] L. Ibanez, W. Schroeder, L. Ng, and J. Cates. *The ITK Software Guide*. Kitware Inc., 2003. 5

[6] P. Jannin, J. Fitzpatrick, D. Hawkes, X. Pennec, R. Shahidi, and M. Vannier. Validation of medical image processing in image-guided therapy. *IEEE Trans. Med. Imag.*, 21(12):1445–1449, 2002. 4

[7] J. Jensen. Field: a program for simulating ultrasound systems. In *the 10th Nordic-Baltic Conference on Biomedical Imaging*, volume 34, pages 351–353, 1996. 4

[8] T. Kadir, A. Zissereman, and M. Brady. An affine invariant salient region detector. In *Proc. ECCV'04*, volume 3021, pages 228–241, 2004. 1, 2

[9] T. Lange, S. Eulenstein, M. Hunerbein, H. Lamecker, and P. Schlag. Augmenting intraoperative 3D ultrasound with preoperative models for navigation in liver surgery. In *Proc. MICCAI'04*, volume 3217, Sep 2004. 1

[10] A. Leroy, P. Mozer, Y. Payan, and J. Troccaz. Rigid registration of freehand 3D Ultrasound and ct-scan kidney images. In *Proc. MICCAI'04*, volume 3216, pages 837–844, 2004. 2

[11] D. G. Lowe. Distinctive image features from scale-invariant keypoints. *International Journal of Computer Vision*, 60(2):91–110, 2004. 1

[12] F. Maes, A. Collignon, and D. Vandermeulen. Multimodality image registration by maximization of mutual information. *IEEE Trans. on Med. Imag.*, 16(2):181–187, 1997. 1

[13] D. Mattes, D. Haynor, H. Vesselle, T. Lewellen, and W. Eubank. PET-CT image registration in the chest using free-form deformations. *IEEE Trans. Med. Imag.*, 22(1):120–128, 2003. 3

[14] S. Ourselin, A. Roche, S. Prima, and N. Ayache. Block matching: A general framework to improve robustness of rigid registration of medical images. In *Proc. MICCAI'00*, volume 1935, 2000. 2

[15] X. Pennec, P. Cachier, and N. Ayache. Tracking brain deformations in time-sequences of 3D US images. *Pattern Recog. Lett.*, 24:801–813, Feb 2006. 1

[16] G. Penney, J. Blackall, M. Hamady, T. Sabharwal, A. Adam, and D. Hawkes. Registration of freehand 3D ultrasound and magnetic resonance liver images. *Med. Image Anal.*, 8(1):81–91, 2004. 2

[17] A. Roche, G. Malandain, N. Ayache, and X. Pennec. Multimodal image registration by maximization of the correlation ratio. *INRIA Research Report*, (3378), 1998. 1, 2

[18] R. Shekhar and V. Zagrodsky. Mutual information-based rigid and nonrigid registration of ultrasound volumes. *IEEE Trans. Med. Imag.*, 21, Jan 2002. 4

[19] C. Stewart, C. Tsai, and B. Roysam. The dual-bootstrap iterative closest point algorithm with application to retinal image registration. *IEEE Trans. Med. Imag.*, 22(11):1379–1394, 2003. 1

[20] C. Studholme, D. Hawkes, and D. Hill. An overlap invariant entropy measure of 3D medical image alignment. *Pattern Recogn.*, 32(11):71–86, 1999. 1

[21] W. Wein, R. Barbara, and N. Nassir. Automatic registration and fusion of ultrasound with CT for radiotherapy. In *Proc. MICCAI'05*, pages 303–311, Oct 2005. 2